

A comparative study of structural, electrical and magnetic properties rare-earth (Dy and Nd)-modified BiFeO₃

Samita Pattanayak · R. N. P. Choudhary ·
Dillip Pattanayak

Received: 23 April 2014 / Accepted: 13 June 2014 / Published online: 8 July 2014
© Springer Science+Business Media New York 2014

Abstract The polycrystalline samples of BiFeO₃ (BFO) and rare earth-modified bismuth iron oxide, Bi_{0.95}R_{0.25}FeO₃ (R = Nd, Dy) (BNFO, BDFO) are prepared by a standard high-temperature solid-state reaction technique. A preliminary x-ray structural analysis is carried out to examine the structural deformation and stability of rare earth-modified BFO. Room temperature surface morphologies and textures of the samples are recorded by a scanning electron microscope, which reveals the uniform distribution of the plate-and rod-shaped grains. Studies of dielectric and electric properties in a wide frequency (1 kHz–1 MHz) and temperature (30–400 °C) ranges using complex impedance spectroscopic method have provided many new results. The dielectric constant is found to be increases, and the tangent loss decreases as compared to BFO. The electrical polarizations (spontaneous and remnant) is found to be enhanced on rare-earth substitutions. Studies of ac conductivity suggest that the samples obey Jonscher's universal power law. The enhancement of magnetization was observed in rare-earth doped samples compared to pure BFO.

1 Introduction

Multiferroic materials have the unique properties with existence of both ferroelectricity and ferromagnetism

phenomenon in a single-phase distorted system. Among all the multiferroic materials available so far, BiFeO₃ (BFO) is the only material known today in which coupling between magnetic and ferroelectric ordering exist at room temperature [1]. This type of effect is known as magneto-electric (ME) coupling effect [2]. As a result, multiferroic materials have become an integral part of recent electronic or advance technology due to their applications in information storage, high-density ferroelectric random access memory (FeRAM), multiple-state memories, magnetic data-storage media, actuators, transducers, sensors, quantum electromagnets, microelectronic devices and spintronics devices [3–5]. The structure of BFO has rhombohedral (i.e., distorted perovskite of ABO₃) with space group R3c [6], where the A-sites could be filled by rare-earth, alkaline earth, alkali or other large ions and the B-sites always filled by transition metal cations. BFO shows simultaneous ferroelectricity [with high Curie temperature ($T_c \sim 1103$ K)], and ferromagnetism [with high Neel temperature ($T_N \sim 630$ K)] in distorted perovskite [7, 8]. Because of the multifunctional applications of ME materials, they simultaneously exhibit spontaneous polarization and spontaneous magnetization. In BFO ferroelectric properties is due to the presence of 6 s lone pair electrons of Bi³⁺ ions, and thus ferromagnetic order is due to Fe³⁺ ions [9]. Unfortunately, the major problems of BFO and other materials of this family are their large leakage current density that limits the applications of the materials. Recently the researchers have developed few new single-phase and composite multiferroic materials with high ordering temperature, high coupling constant, low dielectric loss and low leakage current [10, 11]. The extensive literature survey on BFO structural compounds reveals that a lot of work has been carried out in rare-earth substituted BFO. The present work provides a new insight into the effect of

S. Pattanayak (✉) · R. N. P. Choudhary
Department of Physics, Institute of Technical Education and
Research, Siksha 'O' Anusandhan University,
Khandagiri, Bhubaneswar 751030, Odisha, India
e-mail: samitaphy@gmail.com

D. Pattanayak
Gandhi Institute of Engineering and Technology (GIET),
Gunupur, India

substitution on rare-earth ions ($R = \text{Gd}, \text{Sm}, \text{Dy}, \text{Nd}$ and Pr) at the Bi-site of BiFeO_3 offers the opportunity to optimize several relevance's of the material properties [12–15]. The polycrystalline samples of rare-earth modified bismuth ferrite (i.e., $\text{Bi}_{0.75}\text{R}_{0.25}\text{FeO}_3$; $R = \text{Dy}$ and Nd) (BRFO) were synthesized using a high-temperature solid-state reaction method. Dielectric, Complex impedance spectroscopy has been used to study electrical properties of these compounds. Magnetic analysis has been used to study the magnetic properties of these samples. The grain size and remnant magnetization have been shown to be influenced by rare-earth doping in BFO ceramics.

2 Experimental

The polycrystalline samples of BiFeO_3 , $\text{Bi}_{0.75}\text{R}_{0.25}\text{FeO}_3$ (BRFO) ($R = \text{Dy}$ and Nd) were prepared by using high-purity (>99.9 %) ingredients: Bi_2O_3 , Fe_2O_3 , Dy_2O_3 and Nd_2O_3 (M/s Loba Chemie Pvt. Ltd., India). The materials were first stoichiometrically weighed and mixed thoroughly using agate mortar and pestle in dry medium (i.e., in air atmosphere) for 1 h, and wet medium (methanol) media for about 2 h. The homogeneous mixtures of the above compounds were calcined at optimized temperatures in the range of 780–830 °C in alumina crucible for 4–5 h in air atmosphere. The process of grinding and calcination was repeated until the formation of the compounds was confirmed. The calcined powders were pressed into small disc of diameter = 10 mm and thickness = 1–2 mm at a pressure of $4 \times 10^6 \text{ N/m}^2$ with a binder [polyvinyl alcohol (PVA)]. The pellets were then sintered at different temperature (820–870 °C) for 4 h.

The preliminary structural analysis was performed by means of X-ray diffraction using (XRD; Rigaku Mini flex, Japan). The XRD pattern of the calcined powder was recorded at room temperature with CuK_α ($\lambda = 1.5405 \text{ \AA}$) in a wide range of Bragg angles θ ($20 \leq 2\theta \leq 80^\circ$) at a scanning rate of 3 °/min. The microstructures of sintered pellets were recorded by scanning electron microscopy (SEM; JEOL-JSM, model 6510). For the measurements of electrical properties, a pellet was carefully polished and subsequently painted with high purity Ag-paste on its both sides to work as electrode. The frequency dependence of the capacitance, dissipation factor, phase angle and impedance were measured at different temperatures using a phase sensitive LCR/impedance meter (PSM 1735, N4L). The I-V characteristics of BRFO was measured as a function of voltage (1–100 V) with an interval of 25 °C starting from room temperature (25 °C) up to 400 °C using a programmable electrometer (Keithley, model 6517B). A superconducting quantum interference device (SQUID) magnetometer was used to study the magnetic properties of the materials at room temperature.

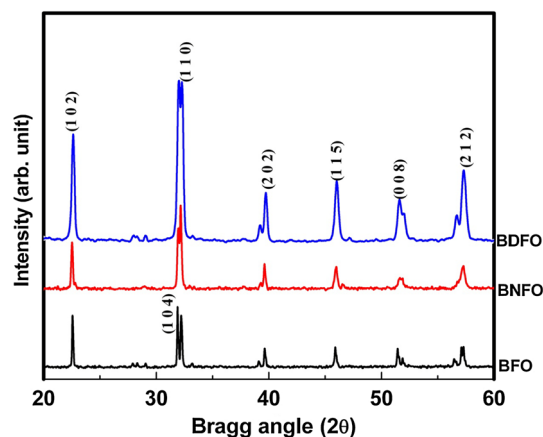


Fig. 1 XRD pattern of BFO, BNFO and BDFO at room temperature

Table 1 Comparison of lattice parameters a , c and volume (\AA^3) with estimated standard deviation (*in parenthesis*) of BiFeO_3 , $\text{Bi}_{0.75}\text{Nd}_{0.25}\text{FeO}_3$ and $\text{Bi}_{0.75}\text{Dy}_{0.25}\text{FeO}_3$ samples

	a	c	c/a	Volume (\AA^3)
BiFeO_3	5.5706 (7)	13.8114 (7)	2.4793	372.96
$\text{Bi}_{0.75}\text{Nd}_{0.25}\text{FeO}_3$	5.5676 (4)	13.7173 (4)	2.4638	368.25
$\text{Bi}_{0.75}\text{Dy}_{0.25}\text{FeO}_3$	5.5161 (2)	13.7944 (2)	2.5007	363.50

3 Results and discussion

3.1 Structural analysis

Figure 1 shows the XRD pattern of BiFeO_3 and $\text{Bi}_{0.75}\text{R}_{0.25}\text{FeO}_3$ ($R = \text{Dy}$ and Nd). All the peaks of the XRD pattern were indexed using standard computer software program 'PowdMult' [13]. The lattice parameters of the samples were analyzed using computer software. From the best agreement between observed (d_{obs}) and calculated (d_{cal}) inter-planer distance d [$\sum (d_{\text{obs}} - d_{\text{cal}} = \text{minimum})$], unit cell lattice parameters and volume of BRFO, structure of the compounds were found to be rhombohedral. There is no indication of change in basic structure of BFO on substituting Nd and Dy. Table 1 shows the comparison of lattice parameters a , c and volume (\AA^3) with estimated standard deviation (*in parenthesis*) of BiFeO_3 , $\text{Bi}_{0.75}\text{Nd}_{0.25}\text{FeO}_3$ and $\text{Bi}_{0.75}\text{Dy}_{0.25}\text{FeO}_3$ samples.

The scanning electron micrograph of BFO, BNFO and BDFO pellets are shown in Fig. 2a–c. It is observed that the grain size of BFO is significantly higher than that of rare-earth doped samples. Grains being smaller, aggregate to form bigger clusters is observed, which is consistent with our XRD study. It is also observed that rare-earth substitution densely less packed samples (i.e. creation of less porosity).

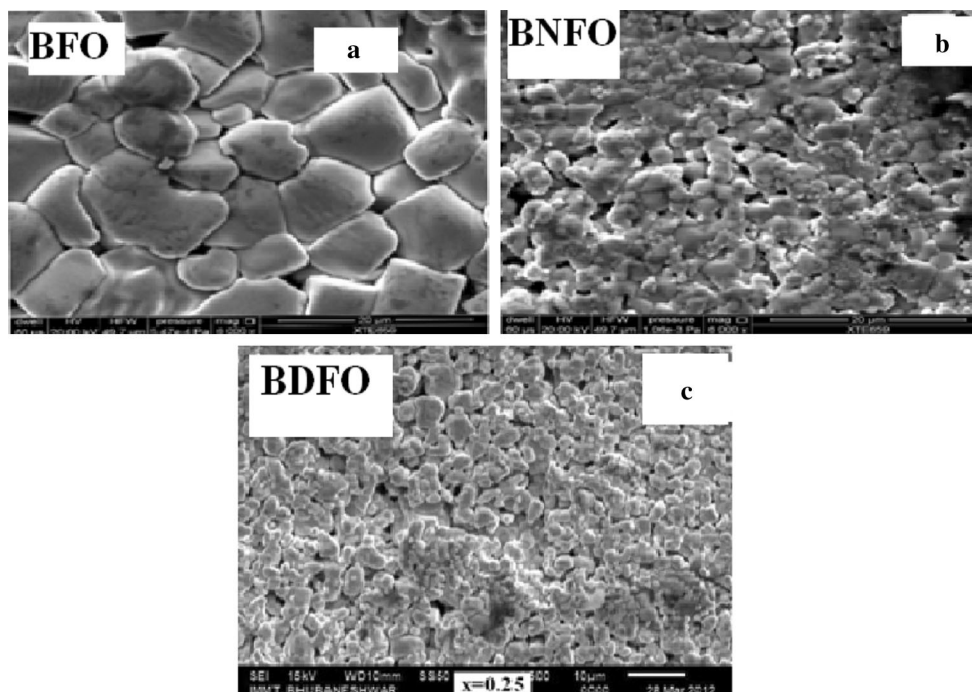


Fig. 2 a–c SEM micrograph for BFO, BNFO and BDFO ceramics

Fig. 3 Variation of ϵ_r and $\tan\delta$ with frequency for BFO, BNFO and BDFO at few selected temperatures

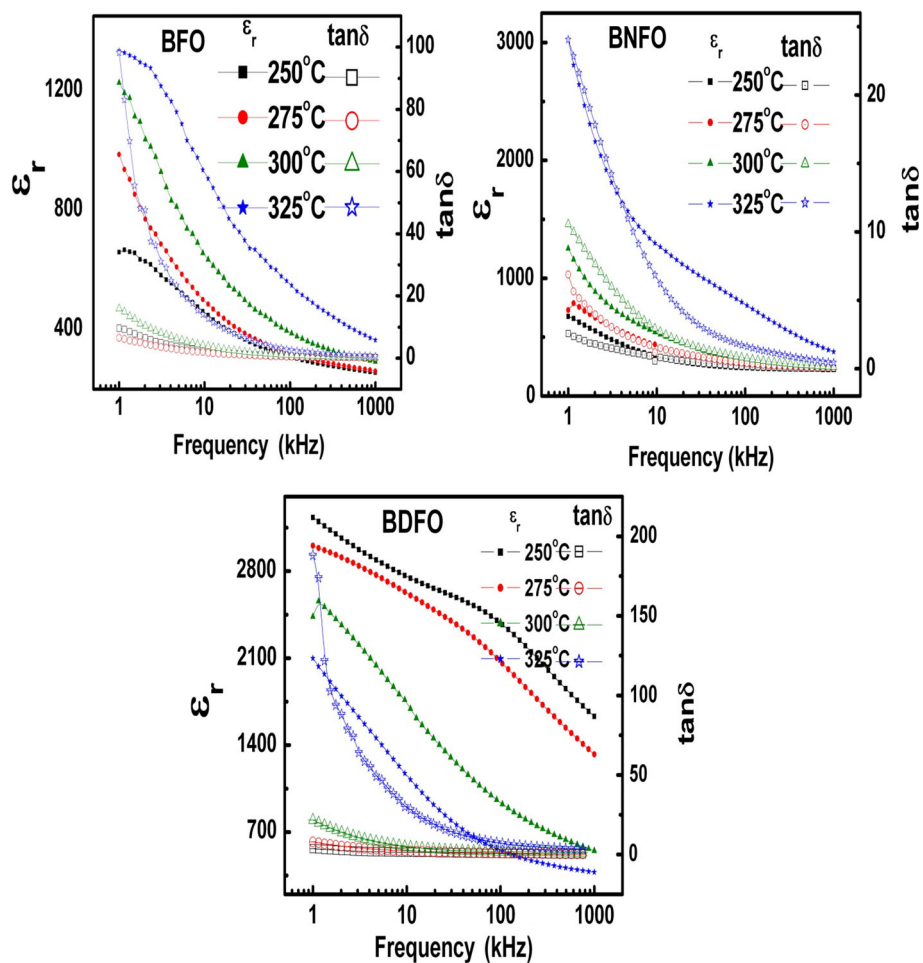
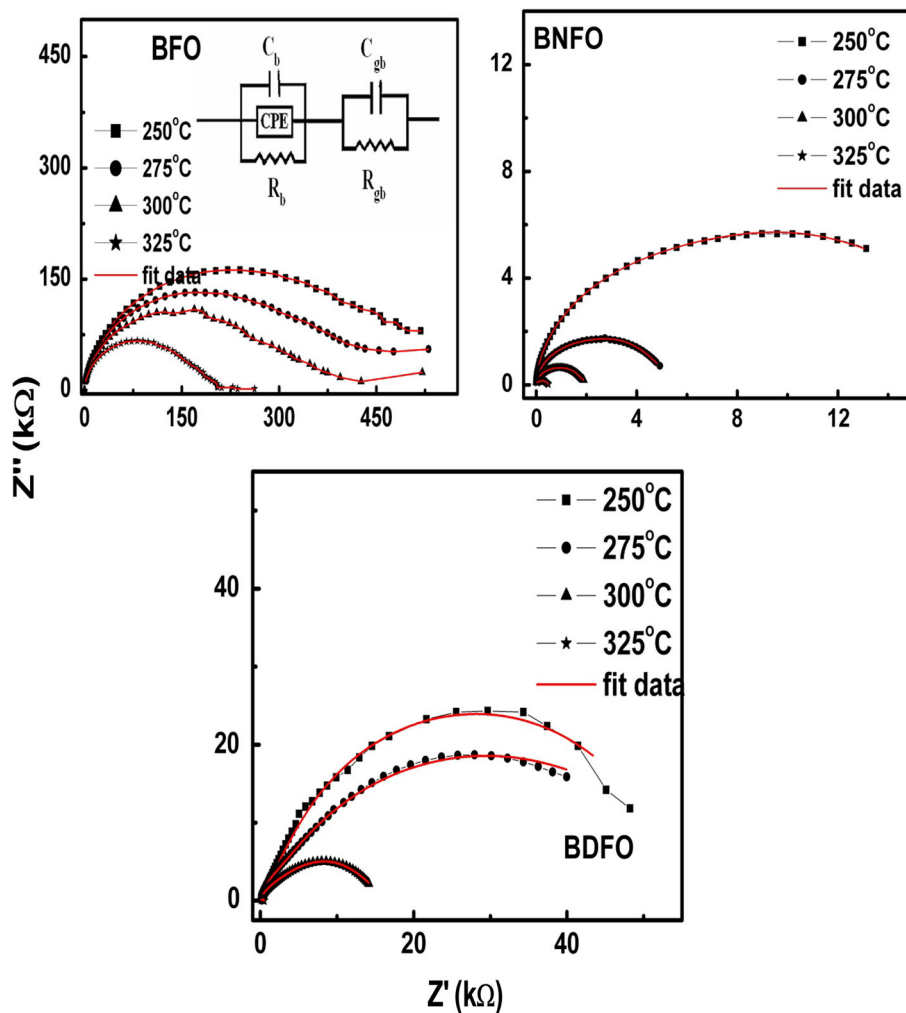


Fig. 4 Variation of Z' with Z'' for BFO, BNFO and BDFO at few selected temperatures



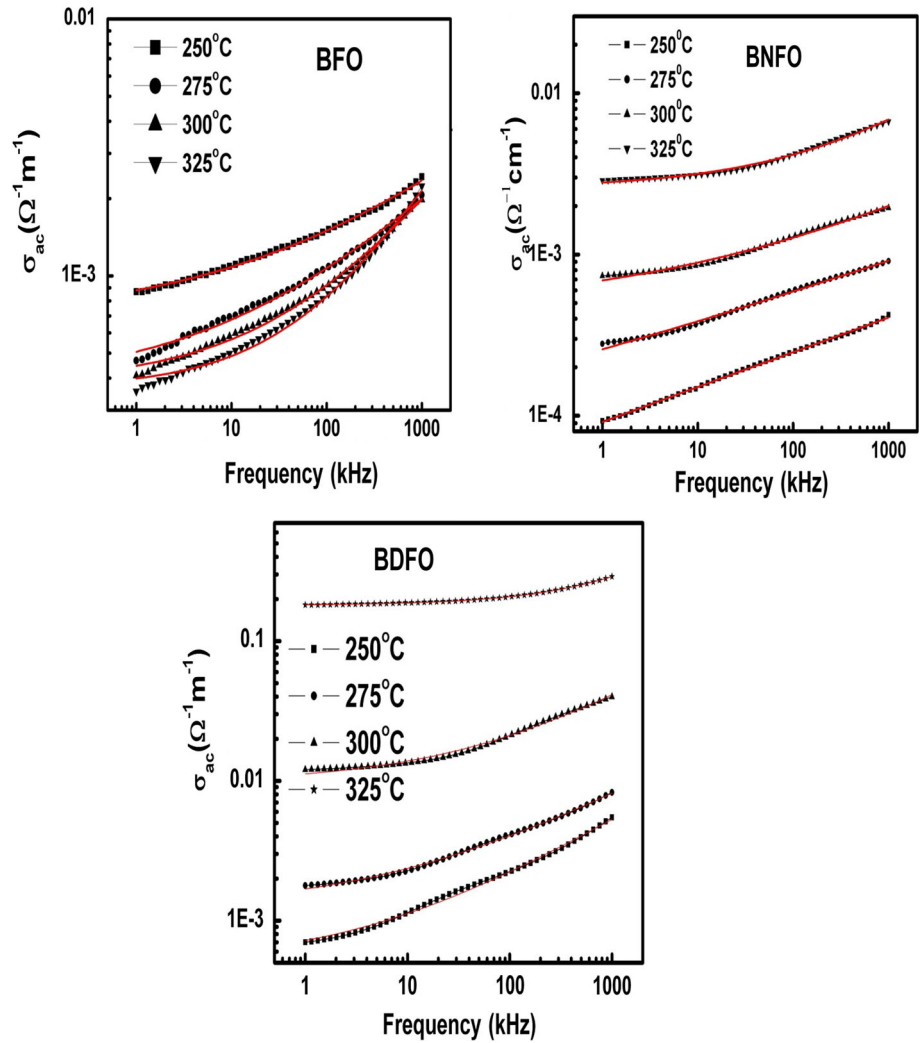
3.2 Electrical properties

Figure 3 shows the frequency dependence of relative permittivity (ϵ_r) and tangent loss ($\tan \delta$) for BFO, BNFO and BDFO at few selected temperatures. It can be observed that all the compounds exhibit dielectric dispersion where dielectric constant decreases rapidly with increasing frequency in the low-frequency region while it approaches almost frequency independent behaviour in the high-frequency region. The dielectric dispersion curve can be explained based on Koop’s theory [14, 15]. This model is based on the Maxwell–Wagner model for the inhomogeneous double structure in determining the dielectric properties of the ferrite materials. The dielectric loss gives the loss of energy from the applied field into the sample. This is caused by domain wall resonance. It is observed from Figure 3 that Nd-modified samples have low dielectric losses as compared to that of BFO and BDFO. The dielectric loss in the oxides of perovskite family is also caused by oxygen vacancies. At lower frequencies the

value of $\tan \delta$ is larger for BDFO as compared to BFO and BNFO. Generally, $\tan \delta$ has very low value at high frequency. It indicates that dipoles with small effective masses (i.e., electrons and ferroelectric domains) mainly contribute to dielectric constant instead of charge defects with large effective masses (i.e., oxygen vacancies). Moreover, the higher values of $\tan \delta$ in BDFO material generally represent large leakage current due to higher conductivity.

Complex impedance spectroscopy (CIS) is an effective and unique method to establish correlation between the electrical properties of dielectric and ionic materials with their microstructures. In this technique, an ac signal is applied across the pellet sample and the output response is measured. The complex impedance data can ideally be analyzed by using an equivalent circuit consisting of two parallel combinations of R (resistance) and C (capacitance) components in a circuit. The frequency dependence of electrical parameters of a material is often represented in terms of complex impedance (Z^*), electric modulus (M^*),

Fig. 5 Variation of ac conductivity (σ_{ac}) with frequency for BFO, BNFO and BDFO at few selected temperatures



complex admittance (Y^*) and complex dielectric constant (ϵ^*) as given below: Complex impedance

$$Z^*(\omega) = Z' - jZ''$$

Where $Z' = R/1 + (\omega CR)^2$ and $Z'' = R^2\omega C/1 + (\omega CR)^2$

$$\epsilon^* = 1/M^* = \epsilon' - j\epsilon''$$

$$\tan\delta = \epsilon''/\epsilon' = M''/M' = -Z'/Z'' = Y''/Y'$$

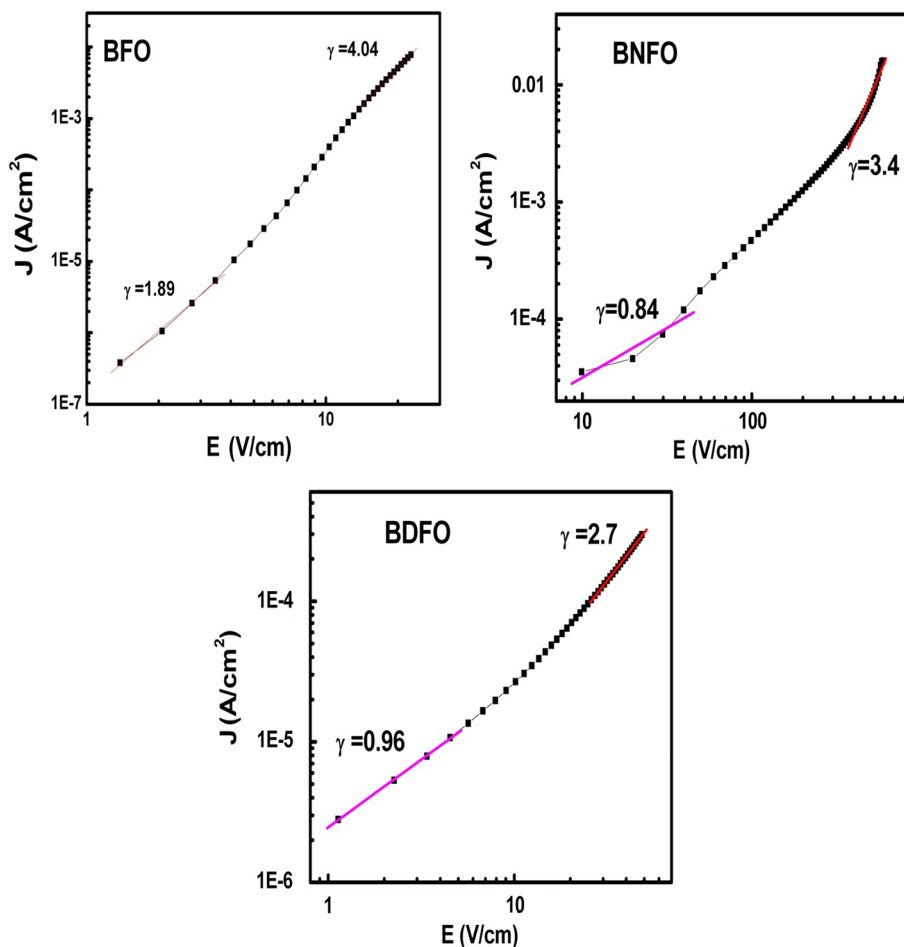
Figure 4 shows the variation of Z'' with Z' (usually referred as Nyquist plot [16]) for BFO, BNFO and BDFO at few selected temperatures. The Nyquist plots typically comprise a single semicircular arc, which is gradually resolved or distorted with rare-earth substituted BFO. The formation of a single arc is mainly due to the grains, and relaxation is due to Debye. For Nd and Dy-substituted BFO, there is a clear indication of formation of second semicircle in the low-frequency region. The formation of second semi-circle is due to grain boundary effect in the material [17]. For ideal Debye—like response, an equivalent circuit consists

of parallel combination of (CQR) and (CR) where Q is said to a constant phase element (CPE).

The admittance of Q is defined as Y (CPE) = $A_0(j\omega)^n = A_0\omega^n + jB_0\omega^n$ where $A = A_0\cos(n\pi/2)$ and $B = A_0\sin(n\pi/2)$, where A_0 and n are frequency independent but temperature dependent parameters. A_0 determines the magnitude of the dispersion. The value of n is in between zero and one ($0 \leq n \leq 1$). For an ideal capacitor $n = 1$ and for ideal resistor $n = 0$ [18].

The presence of non-semicircle, asymmetric or distorted semi-circle suggests the existence of non-Debye type of relaxation in the samples [19]. For an ideal Debye-type relaxation, a perfect semicircle with its center at Z' -axis is observed. The above observation clearly suggests that the studied materials do not obey Debye-type of relaxation. The observed depressed semicircular arcs having center lies below the real impedance (Z') axis is due to the presence of distributed phase elements. The relaxation process associated with this observation is non-ideal in nature. This non-ideal behaviour may be originated from the several

Fig. 6 Variation of current density versus electric field for BFO, BNFO and BDFO at room temperature



factors such as grain orientation, grain size distribution, grain boundaries, atomic defect distribution, and stress-strain phenomena [20]. The intercept of each semi-circle on real Z' -axis gives the value of bulk and grain boundary contributions in the resistance. The decrease in area of the semicircles is observed on increasing temperature in all the compounds. It reveals that the bulk relaxation of the sample varies with temperature in the studied frequency range. The value of bulk resistance (R_b) decreases with rise in temperature as well as Nd and Dy-modified BFO and indicate the presence of negative temperature coefficient of resistance (NTCR), as observed in semiconductors [21, 22]. The semi-circle of impedance spectra have a characteristic peak occurring at a particular frequency usually referred as relaxation frequency (f_r). It can also be expressed as $\omega_r R_b C_b = 1$ and thus $f_r = 1/2\pi R_b C_b$. The relaxation time due to bulk effect (τ_b) has been calculated using the equation $\omega_r \tau_b = 1$ or, $\tau_b = 1/2\pi f_r$. The impedance value of BNFO and BDFO decreases, which shows more conductivity contribution for rare-earth modified BFO.

Figure 5 shows the frequency dependence of ac conductivity for BFO, BNFO and BDFO at few selected

temperatures. The ac conductivity was calculated using an empirical dielectric relation:

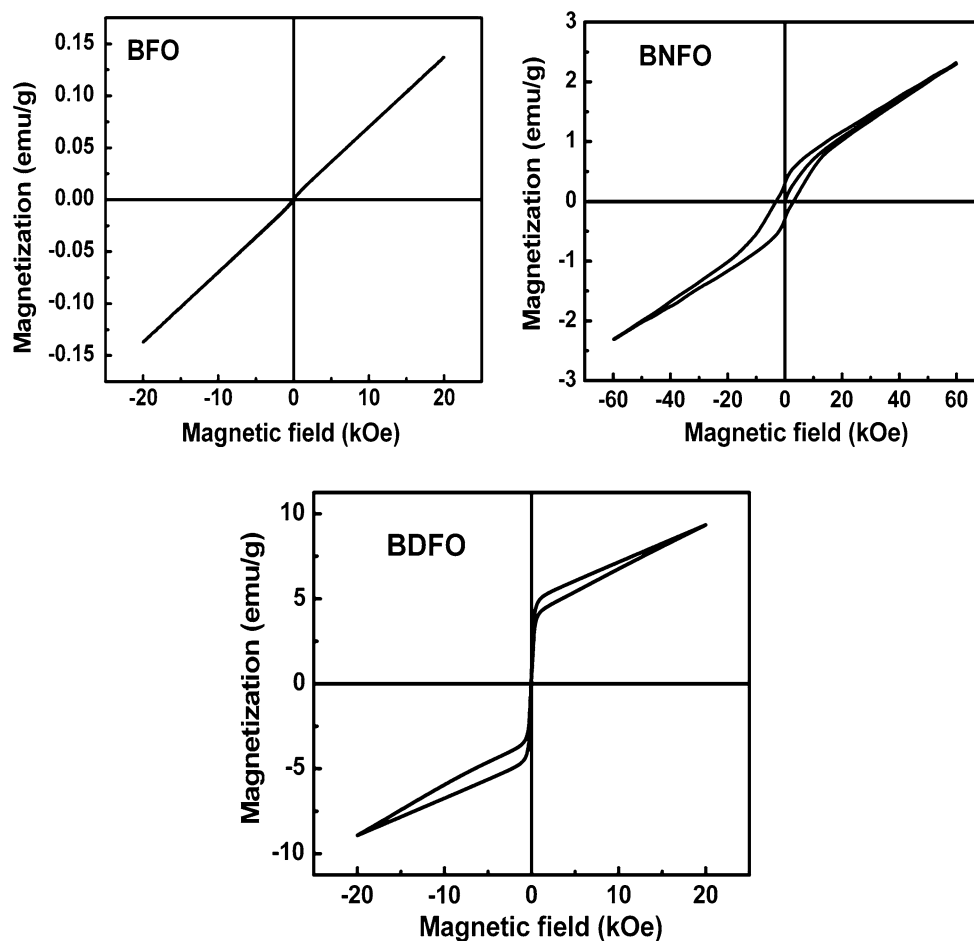
$$\sigma_{ac} = \omega \epsilon_r \epsilon_0 \tan \delta$$

(ω = angular frequency, ϵ_0 = vacuum permittivity). Study of ac conductivity is important to understand the frequency dependence of electrical transport properties of the material. The frequency dependence of ac conductivity is explained using Jonscher's power law [23],

$$\sigma_T(\omega) = \sigma(o) + \sigma_1(\omega) = \sigma_o + a\omega^n$$

$\sigma_T(\omega)$ is the total ac conductivity, $\sigma(o)$ is the dc conductivity term (i.e., independent of frequency), $\sigma_1(\omega)$ is the dispersive component of ac conductivity, n is frequency independent but temperature dependent parameter. The value of n lies between zero and one. According to Jonscher's power law, the relaxation is due to the mobile charge carriers. When a mobile charge carrier jumps from its original position to a new-site, which is in a state between two potential energy minima. If $n < 1$, the motion is translational, and $n > 1$ the motion is localized [24]. From Fig. 5, it is evident that the magnitude of ac conductivity rises with rise in temperature (i.e., thermally

Fig. 7 M–H hysteresis loops for BFO, BNFO and BDFO ceramics at room temperature



activated process). This is in good agreement with the observation made from the impedance variation with frequency. At high temperature (325 °C) and at low frequency domain, a plateau is observed indicating presence of dc conductivity. The plateau region extends to higher frequencies with increasing temperature. This feature is compatible with the development of a delocalized or low-localization conduction mechanism. In the dispersion region, there is a frequency at which a change in the slope of conductivity spectrum appears. This is conventionally known as the hopping frequency (ω_p). The values of hopping frequencies as observed increased with the rise of temperature suggesting a possible enhancement in the carrier hopping rate of the mobile charge carriers with rise in temperature. The deviation from low frequency plateau at lower temperatures may be assigned to electron conduction through quantum mechanical tunneling between localized states. The power law regime of all the spectra is much less temperature dependent than the dc conductivity. At low temperatures σ_{ac} is found to obey a power relation. These indicate that the transport mechanism is due to hopping of carriers via localized electron states [25].

Figure 6 shows the current density versus electric field for BFO, BNFO and BDFO at room temperature. The value of current density increases rapidly on increasing the electric field. It is found that Nd, Dy-modified BFO has high leakage current as compared to that of BFO. The increase of leakage current density in BNFO and BDFO is attributed to the effective reduction of the defect by the substituting Nd and Dy ions into the BFO. In the low-field region, curves of BNFO and BDFO obey the Ohmic-type of conduction behaviour ($J \propto E^\gamma$: $\gamma \sim 1$) [26]. In the high-electric field region, the curve obeys Child's law ($J \propto E^\gamma$: $\gamma > 1$). Thus, in the high-electric field and high-temperature region, the conduction mechanism may be considered as combination of space charge limited, Schottky and Frenkel-Poole [27].

3.3 Magnetic properties

The field dependence of magnetization of BFO, BNFO and BDFO samples were measured between the fields of -2.5 – 2.5 T at room temperature using (SQUID). Figure 7 shows the M–H hysteresis loops of all the samples. The M–H loops indicate that the magnetic properties of doped

samples are much more enhanced as compared to that of BFO. BFO has non-zero remnant magnetization (M_r) of the value of 4.72×10^{-4} emu/g at a coercive magnetic field (H_c) of 4.24×10^{-6} kOe. This is because BFO is known to be anti-ferromagnetic having a G-type magnetic structure but has a residual magnetic moment due to a canted spin structure (weak ferromagnetic) [28]. However, the switching behaviour as observed in BDFO, at low fields is the most interesting and exchange observations of the field dependence of magnetization which occurs at room temperature. It is noted that the enhancement of magnetic moment or magnetization is also accompanied with the decrease of grain size as evident from our SEM micrograph [29]. From the above Fig. 7, magnetization value is highest for BDFO sample because the effective Bohr magneton of Dy ($9.8\mu_B$) is larger as compared to that of BFO and BNFO.

4 Conclusion

The polycrystalline samples BFO, BNFO and BDFO were prepared by a solid-state reaction method. The XRD analysis of the samples suggests that there is no effect on crystal structure for Nd and Dy-modified BFO. The SEM micrographs showed that on substituting Nd, Dy- content in BFO, the grain size of the samples decreases and distributed uniformly. We also observed a remarkable change in the dielectric and conduction properties of the Nd, Dy-modified BFO. The impedance studies exhibit the presence of grain (bulk) and grain boundary effects, and existence of a negative temperature coefficient of resistance (NTCR) in the materials. It has been observed that Dy-substitution in BFO enhances the ferromagnetic properties and exhibits anti-ferromagnetic behavior of the samples at room temperature.

References

1. W. Eerenstein, N.D. Mathur, J.F. Scott, Multiferroic and magnetoelectric materials. *Nature (London)* **442**, 759 (2006)
2. M. Li et al., Room temperature ferroelectric, ferromagnetic and magnetoelectric properties of Ba-doped BiFeO₃ thin film. *J. Phys. D Appl. Phys.* **40**, 1603 (2007)
3. N.A. Hill, Why are there so few magnetic ferroelectrics? *J. Phys. Chem. B* **104**, 6694 (2000)
4. M. Fiebig, Revival of the magnetoelectric effect. *J. Phys. D* **38**, R123 (2005)
5. B. Yu, M. Li, J. Liu, D. Guo, L. Pei, X. Zhao, Effects of ion doping at different sites on electrical properties of multiferroic BiFeO₃ ceramics. *J. Phys. D Appl. Phys.* **41**, 065003 (2008)
6. A.A. Saad, W. Khan, P. Dhiman, A.H. Naqvi, Structural, optical and magnetic properties of perovskite (La_{1-x}Sr_x) (Fe_{1-x}Ni_x) O₃, ($x = 0.0, 0.1$ & 0.2) nanoparticles. *Electron. Mater. Lett.* **9**, 77 (2013)
7. G.A. Smolenskii, I. Chupis, Ferroelectromagnets. *Sov. Phys. Usp.* **25**, 475 (1982)
8. F. Kubel, H. Schmid, Growth, twinning and etch figures of ferroelectric/ferroelastic dendritic BiFeO₃ single domain crystals. *J. Cryst. Growth* **129**, 515 (1993)
9. C.W. Nan, M.I. Bichurin, S. Dongb, D. Viehland, Multiferroic magnetoelectric composites: historical perspective, status, and future directions. *J. Appl. Phys.* **103**, 031101 (2008)
10. Swagatika Dash, R. Padhee, Piyush R. Das, R. N. P. Choudhary, Enhancement of dielectric and electrical properties of NaNbO₃-modified BiFeO₃, *J Mater Sci: Mater Electron* DOI 10.1007/s10854-013-1249-4
11. M. Mandal, M. Mandal, S.P. Duttagupta, V.R. Palkar, Study of multiferroic Bi_{0.7}Dy_{0.3}FeO₃ based tunable ring inductor. *J. Phys. D Appl. Phys.* **46**, 325001 (2013)
12. P.C. Sati, M. Arora, S. Chauhan, S. Chhoker, M. Kumar, Structural, magnetic, and optical properties of Pr and Zr codoped BiFeO₃ multiferroic ceramics. *J. Appl. Phys.* **112**, 094102 (2012)
13. N.K. Verma, G.S. Lotey, Structural, magnetic, and electrical properties of Gd-doped BiFeO₃ nanoparticles with reduced particle size. *J. Nanopart. Res.* **14**, 742 (2012)
14. D. Maurya, H. Thota, A. Garg, B. Pandey, H.C. Verma, Magnetic studies of multiferroic Bi_{1-x}Sm_xFeO₃ ceramics synthesized by mechanical activation assisted processes. *J. Phys. Cond. Matter* **21**, 026007 (2009)
15. S. Zhang, L. Wang, Y. Chen, D. Wang, Y. Yao, Y. Ma, Observation of room temperature saturated ferroelectric polarization in Dy substituted BiFeO₃ ceramics. *J. Appl. Phys.* **111**, 074105 (2012)
16. E. W. POWD, An interactive Powder diffraction data interpretation and indexing program, ver 2.1, School of Physical Science, Finders University of South Australia, Bedford Park, S.A. 5042, Australia
17. C.G. Koop's, *Phys. Rev.* **83**, 127 (1951)
18. K.W. Wagner, Zur theorie der unvollkommenen dielektrika. *Ann. Phys.* **40**, 817 (1913)
19. B. Yeum, Z. Simpwin Version 2.00, Echem software Ann Arbor, MI, USA
20. T.S. Irvine, D.C. Sinclair, A.R. West, Electroceramics: characterization by impedance spectroscopy. *Adv. Mater.* **2**, 132 (1990)
21. J. Ross Macdonald, Note on the parameterization of the constant-phase admittance element. *Solid State Ion.* **13**, 147 (1984)
22. A.R. West, D.C. Sinclair, N. Hirose, Characterization of electrical materials, especially ferroelectrics, by impedance spectroscopy. *J. Electroceram.* **1**, 65 (1997)
23. I.G. Ismailzade, X-ray diffraction study of phase transitions in the BiFeO₃-Pb (Fe_{0.5}Nd_{0.5}) O₃ system. *Kristallografiya* **13**(3), 431–434 (1968)
24. R.N.P. Choudhary, D.K. Pradhan, C.M. Tirado, G.E. Bonilla, R.S. Khatiyar, Effect of La substitution on structural and electrical properties of Ba (Fe_{2/3}W_{1/3}) O₃ nanoceramics. *J. Mater. Sci.* **42**, 7423 (2007)
25. C. Karthik, K.B.R. Verma, Dielectric and AC conductivity behavior of BaBi₂Nb₂O₉ ceramics. *J. Phys. Chem. Solids* **67**, 2437 (2006)
26. A.K. Jonscher, *Nature* **267**, 673 (1997)
27. S. Bhattachaeeya, S.S.N. Bharadwaja, S.B. Krupanidhi, *J. Appl. Phys.* **88**, 4294 (2000)
28. A. Mishra, S.N. Choudhary, R.N.P. Choudhary, V.R.K. Murthy, K. Prasad, *J. Mater. Sci. Mater. Electron.* **23**, 185–192 (2012)
29. T. Kawae, Y. Terauchi, H. Tsuda, M. Kumeda, A. Morimoto, *Appl. Phys. Lett.* **94**, 112904 (2009)